

# Dual-Color Optical Recording of Bioelectric Potentials by Polymer Electrochromism

Yuecheng Zhou, Erica Liu, Yang Yang, Felix S. Alfonso, Burhan Ahmed, Kenneth Nakasone, Csaba Forró, Holger Müller,\* and Bianxiao Cui\*



Cite This: *J. Am. Chem. Soc.* 2022, 144, 23505–23515



Read Online

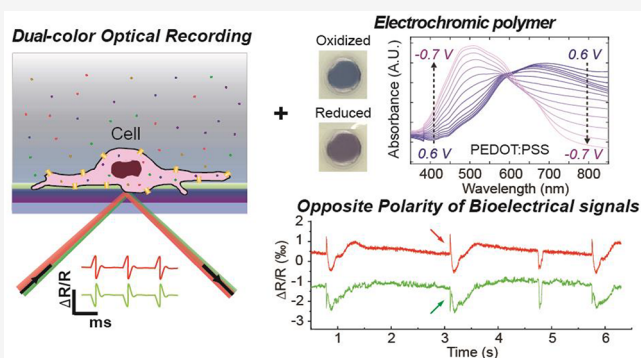
ACCESS |

Metrics & More

Article Recommendations

Supporting Information

**ABSTRACT:** Optical recording based on voltage-sensitive fluorescent reporters allows for spatial flexibility of measuring from desired cells, but photobleaching and phototoxicity of the fluorescent labels often limit their sensitivity and recording duration. Voltage-dependent optical absorption, rather than fluorescence, of electrochromic materials, would overcome these limitations to achieve long-term optical recording of bioelectrical signals. Electrochromic materials such as PEDOT:PSS possess the property that an applied voltage can either increase or decrease the light absorption depending on the wavelength. In this work, we harness this anticorrelated light absorption at two different wavelengths to significantly improve the signal detection. With dual-color detection, electrical activity from cells produces signals of opposite polarity, while artifacts, mechanical motions, and technical noises are uncorrelated or positively correlated. Using this technique, we are able to optically record cardiac action potentials with a high signal-to-noise ratio, 10 kHz sampling rate, >15 min recording duration, and no time-dependent degradation of the signal. Furthermore, we can reliably perform multiple recording sessions from the same culture for over 25 days.



## INTRODUCTION

Electrophysiological recordings allow us to detect voltage fluctuations across the cell membrane, such as action potentials of cardiomyocytes and neurons. Reliable detection of these electrical signals is important for understanding cardiac proarrhythmia,<sup>1</sup> deciphering the information encoded within neuronal networks,<sup>2</sup> and developing brain–machine interfaces.<sup>3</sup> In the past decade, optical recording of bioelectrical activities has gathered significant interest. Compared to electrode-based recording methods, optical recording uses voltage-dependent fluorophores to convert bioelectrical signals into optical readouts. Optical recording avoids complex electrical wiring, which often compromises the transparency of the substrate. It offers spatial flexibility in selecting target cells, high spatial resolution for subcellular detection, and the potential to image all cells in a local neuronal network.<sup>4,5</sup> Genetically encoded fluorescent reporters also offer unique advantages such as selective expression in a desired subset of neurons to enable *in vivo* voltage imaging.<sup>6</sup> Nevertheless, fluorescent indicators such as calcium indicators have slow temporal dynamics and thus are unable to resolve fast action potential spikes.<sup>7–9</sup> Voltage-dependent reporters such as potentiometric dyes<sup>10</sup> or fluorescent proteins<sup>11</sup> usually have faster temporal dynamics but lower contrast brightness when recording at a high frame rate of 500–1000 frames/s. At such a

high frame rate, these probes have limited recording duration, seconds to minutes, due to photobleaching,<sup>12</sup> phototoxicity,<sup>13</sup> or perturbations to the membrane capacitance.<sup>14,15</sup>

Label-free optical electrophysiology seeks to avoid these limitations that are associated with fluorescent labels. In the past decade, several label-free optical recording methods have been developed to detect bioelectrical potentials. For example, nitrogen-vacancy color centers of a thin diamond layer were used to detect the nuanced magnetic field accompanied by the electrical signals of excited worm and squid giant axons.<sup>16</sup> Field-sensitive optical transitions in graphene have been used to convert electrical signals into reflectance changes to detect spontaneous action potentials from whole chicken hearts.<sup>17</sup> Intrinsic optical properties of cells such as light scattering or membrane deformations can be modulated by membrane potentials,<sup>18</sup> although these properties are indirect readouts and can be modulated by cellular mechanisms other than action potentials.<sup>19,20</sup> Recently, we demonstrated that Electro-

Received: September 24, 2022

Published: December 16, 2022



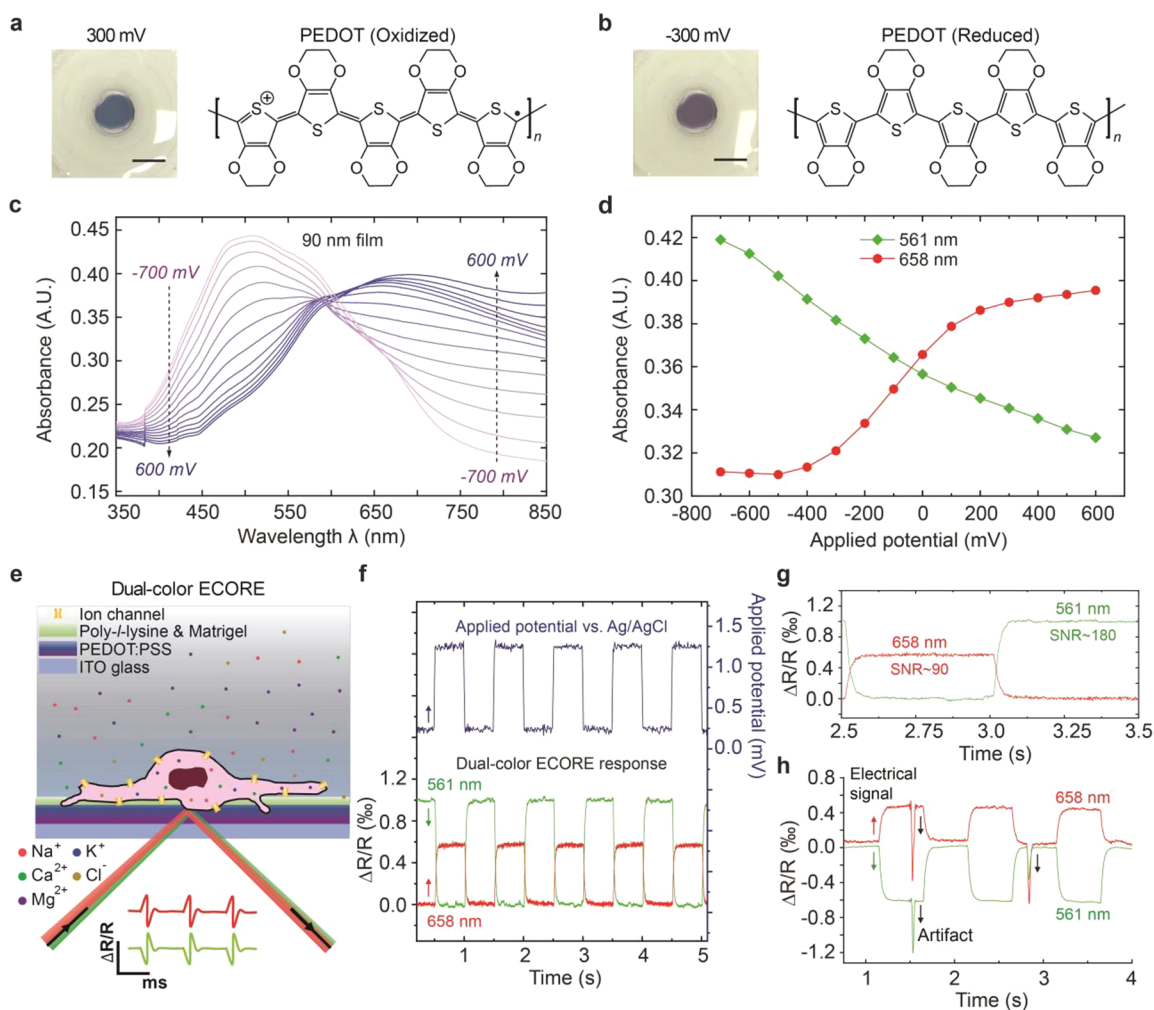


**Figure 1.** Dual-color ElectroChromic Recording (ECORE) using PEDOT:PSS thin films. (a and b) A PEDOT:PSS thin film at (a) + 300 mV potential (oxidized state, blue color) and (b) −300 mV potential (reduced state, purple color) and the respective molecular structures. Scale bar = 5 μm. (c) Ultraviolet–visible (UV–vis) spectra of a 90 nm-thick PEDOT:PSS film under different applied voltages from +600 to −700 mV with a 100 mV step. (d) Absorbances at 561 nm (green) and 658 nm (red) change in opposite directions as a function of applied voltage. (e) Schematic drawing of a cell cultured on a PEDOT:PSS thin film. Two probing lasers with overlapping optical paths are total-internally reflected at the interface. The light reflection,  $R$ , is sensitive to the spectral shift induced by cell electrical activities. (f) When a train of 1 mV square wave voltages is applied to the PEDOT:PSS film using a potentiostat (top panel), the corresponding reflectance changes,  $\Delta R/R$ , of the two channels (561 nm in green, 658 nm in red) change in opposite directions (bottom panel). The arrows indicate the direction of the optical response. (g) Zoom-in traces of the 561 nm channel (green) shows a signal-to-noise ratio (SNR) of  $\sim 180$  and the 658 nm channel (red) shows an SNR of  $\sim 90$ . (h) Artifacts (likely dust particles) result in the same-direction spikes in the two channels, which is in contrast to opposite-direction changes in response to electrical signals.

Chromic Optical Recording (ECORE) converts bioelectrical signals into optical readout by harnessing the electrochromic property<sup>21</sup> of  $\pi$ -conjugated polymer poly(3,4-ethylenedioxythiophene) polystyrenesulfonate (PEDOT:PSS) thin films.<sup>22</sup> ECORE is able to record spontaneous action potentials from individual cardiomyocytes and neurons. However, the recording is susceptible to vibrations or dust particles in the optical path, which could generate noises or artifacts with orders of magnitude comparable to the real bioelectrical signal.

Here, we develop a dual-color ECORE that significantly suppresses artifacts and improves the signal-to-noise ratio. A unique property of PEDOT:PSS is that, in response to an electrical signal, its optical absorption can change in opposite directions (increase or decrease) under different wavelengths. This is in contrast to artifacts from environmental vibration, cellular mechanical motion, and electrical and technical noises that are common-mode and change in the same direction in

both color channels. We demonstrate that dual-color ECORE records individual action potentials with excellent signal-to-noise ratios. These recordings do not suffer from photobleaching or phototoxicity and can record for >15 min at 10 kHz for each recording session with repeated recording sessions over 25 days.

## RESULTS

**Dual-Color ECORE Using Electrochromic PEDOT:PSS Thin Films.** Poly(3,4-ethylenedioxythiophene) polystyrenesulfonate (PEDOT:PSS) thin films were prepared by electropolymerization of 3,4-ethylenedioxythiophene (EDOT) monomers mixed with polystyrenesulfonate (PSS) on indium–tin–oxide (ITO) coated glass substrates. The film thickness is proportional to the electropolymerization time (Figure S1a). The film shows grain-like surface morphology<sup>23</sup> with a domain size between 50 and 100 nm (Figure S1b). The electro-

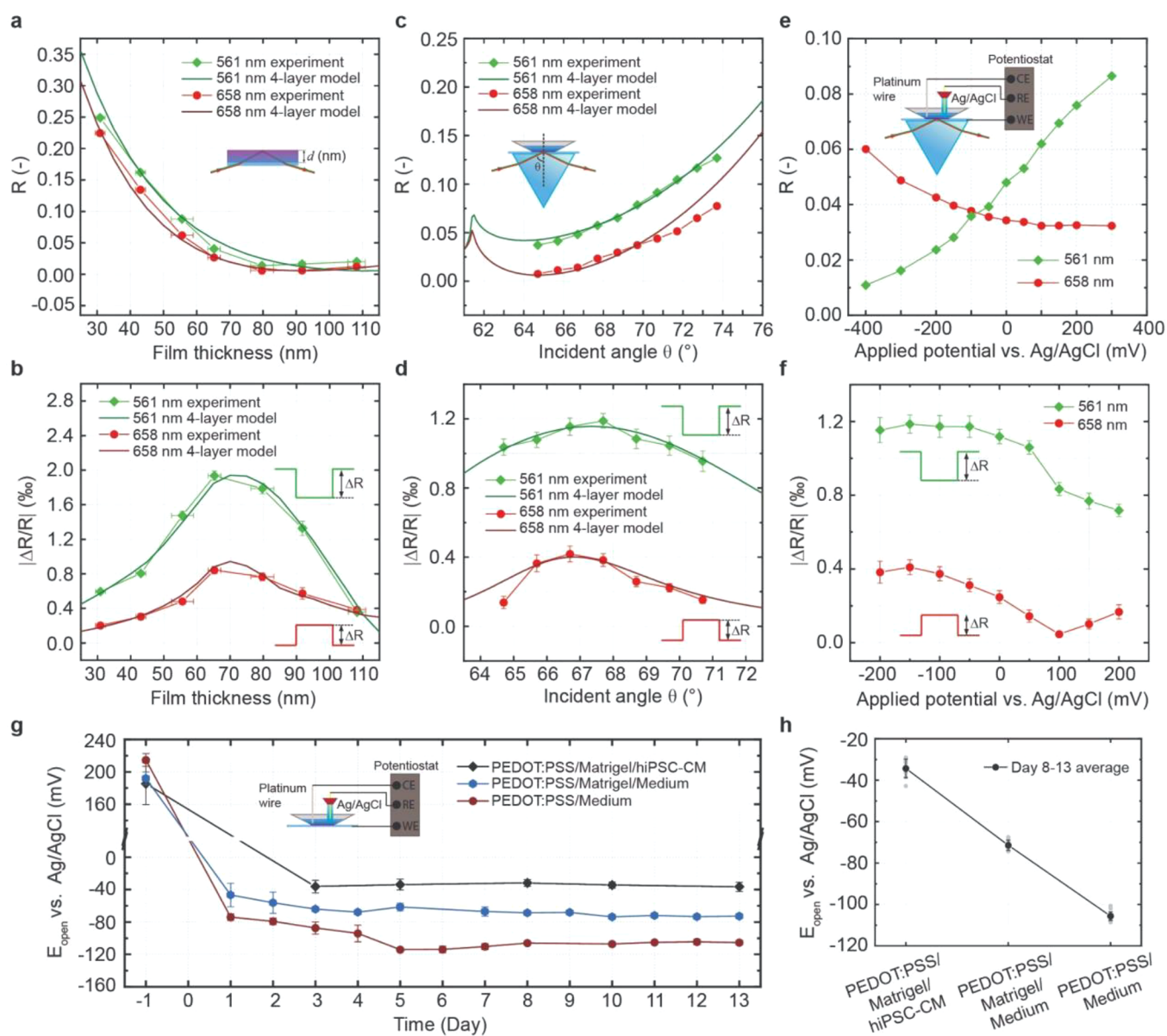


**Figure 2.** Characterization of the dual-color ECORE. (a) Measured and modeled reflectance  $R$  at two color channels with respect to the thickness of PEDOT:PSS thin film. (b) Measured and modeled absolute value of fractional reflectance change  $|\Delta R/R|$  of PEDOT:PSS thin film in response to a 1 mV, 1 Hz applied square-wave potential with respect to different film thicknesses. (c) Measured and modeled reflectance  $R$  with respect to different incident angles. (d) Measured and modeled absolute value of fractional reflectance change  $|\Delta R/R|$  in response to a 1 mV, 1 Hz applied square-wave potential with respect to different incident angles. (e) Measured reflectance  $R$  at different bias potentials. (f) Measured absolute value of fractional reflectance change  $|\Delta R/R|$  in response to a 1 mV, 1 Hz applied square-wave potential at different bias potentials. (g) Measured open-circuit potential,  $E_{\text{open}}$ , with respect to the Ag/AgCl reference electrode, of PEDOT:PSS thin films at four different conditions: (1) freshly made film (day -1); (2) films exposed to culture medium for 1–13 days; (3) films coated with Matrigel and then exposed to culture medium for 1–13 days; (4) films coated with Matrigel and then plated with cardiomyocyte cells for 1–13 days; Day 0 indicates the day when cells were seeded or cell culture media was added to the film. (h) Stabilized  $E_{\text{open}}$  under different conditions. All error bars indicate two standard deviations.

polymerized PEDOT:PSS film changes color when external electrical voltages are applied. The film appears blue in the oxidized (or doped) state at 300 mV (Figure 1a) and purple in the reduced (or undoped) state at -300 mV (Figure 1b). The ultraviolet–visible (UV–vis) spectra of a 90 nm PEDOT:PSS thin film show a clear voltage-dependent shift (measured with respect to the Ag/AgCl reference electrode in an aqueous cell) (Figure 1c). These spectra are independent of the film thickness (Figure S2). The spectra show a peak absorbance at  $\sim 513$  nm for PEDOT in the reduced state, which is a characteristic of the  $\pi$ – $\pi^*$  interband transition. By extrapolat-

ing the onset of the  $\pi$ – $\pi^*$  transition to the background absorbance baseline,<sup>24,25</sup> the band gap energy  $E_g$  of the electropolymerized PEDOT:PSS film is estimated to be  $\sim 1.7$  eV (Figure S3a). The formal potential  $E_f$  is determined to be  $\sim -180$  mV, where the peak absorbance reaches midway of its extrapolated maximum and minimum value (Figure S3b).

As the film is further oxidized, the peak absorbance at  $\sim 513$  nm decreases and gives rise to a polaronic band at  $\sim 700$  nm. Compared to previously reported PEDOT films synthesized via electropolymerization,<sup>26,27</sup> our PEDOT:PSS film exhibits slightly blue-shifted peak absorbance and polaronic band, likely

due to a different PSS composition and the formation of shorter PEDOT chains that lead to a decreased  $\pi$ -conjugation length.<sup>28–30</sup> The UV–vis spectra exhibit a striking feature of an isosbestic point at  $\sim 600$  nm (optical absorption changes minimally with the voltage), with the optical absorption for  $\lambda < 600$  nm decreasing with the increasing voltage while the optical absorption for  $\lambda > 600$  nm increases with the increasing voltage. We chose 561 and 658 nm as we have high-quality lasers at these wavelengths. Figure 1d shows film absorptions at these two wavelengths under applied voltages, which show voltage-dependent changes in opposite directions in the range  $-200$  to  $100$  mV.

To detect bioelectrical signals that are on the orders of tens to hundreds of microvolts, we built an ultrasensitive optical platform based on prism-coupled total internal reflection configuration and differential photodetection (Experimental Methods and Figure S4a). Detecting the reflected rather than the transmitted light keeps the upper surface of the sample free for imaging or inserting counter/reference electrodes for calibration and avoids spurious signals resulting from light scattering from cells or the lipid–air interface.<sup>27</sup> Differential photodetection is used to reduce common-mode fluctuations such as vibrations or laser instabilities. With less than  $100$  nm in their wavelength difference, the two probing lasers of 561 and 658 nm are coupled into the same single-mode optical fiber and focused to a  $25 \mu\text{m}$  spot on the surface of the PEDOT:PSS film through the prism using achromatic lenses and optics (Figure 1e and Figure S4b). In this way, the two wavelengths independently probe the same region of interest in the film, allowing for two independent recording channels.

When applying a train of  $1$  mV,  $1$  Hz square waves to the PEDOT:PSS film (Figure 1f), we observe clear voltage-induced changes in reflectance in both channels (Figure 1f and Figure S5). The fractional reflectance changes,  $\Delta R/R$ , of the two-color channels move in opposite directions in response to the same voltage jump. The  $10\%$ – $90\%$  rise time is measured at  $\tau_r = 31.6$  ms for both channels, as expected since two optical responses arise from the same source. We have previously measured that the temporal response,  $\tau_r$ , scales with the square root of the sensing area,<sup>22</sup> which is consistent with the resistor-capacitor circuit (RC circuit) model for microelectrodes.<sup>31</sup> The PEDOT:PSS film used in this measurement had an area of  $28.3 \text{ mm}^2$ . For a cell with an area of  $\sim 400 \mu\text{m}^2$ , we expect the temporal response time to be  $\sim 0.12$  ms.

At  $10$  kHz of recording frequency, we measured a signal-to-noise ratio (SNR) of  $\sim 180$  for the 561 nm channel and an SNR of  $\sim 90$  for the 658 nm channel in response to a  $1$  mV square wave (Figure 1g). When combining the signal of two channels with a weighted average (Experimental Methods), the SNR is improved to  $>200$  for a  $1$  mV applied voltage. As the optical response is linearly dependent on the applied voltage,<sup>22</sup> we estimate the detection limit of our system to be  $\sim 5 \mu\text{V}$ . Finally, when artifacts were observed during recording, they induce the same-direction changes in two channels, which is in contrast to the opposite-direction changes induced by electrical signals (Figure 1h). This unique feature of dual-color ECORE distinguishes electrical signals from artifacts and noises.

**Characterization and Modeling of Dual-Color ECORE under Cell-Free Conditions.** We experimentally measured how film thickness, incident angle of the laser beam, and the applied bias potential to the film separately affect the performance of ECORE in two different color channels. To further understand the system, we also modeled the light

reflection in the system using a four-layer (glass/ITO/PEDOT/water) reflectivity model<sup>22</sup> and compared the results with experimental data. For modeling parameters, the complex refractive index of PEDOT:PSS,  $1.41 + i0.23$  at 561 nm and  $1.40 + i0.35$  at 658 nm, are experimentally determined by ellipsometry,<sup>22</sup> which have slightly different values at these two wavelengths due to different absorptions. Details of the modeling are included in the Supporting Information.

The total reflectance  $R$  decreases monotonically with film thickness ranging from  $30$  to  $110$  nm for both channels (Figure 2a). However, the signal,  $\Delta R/R$ , in response to a  $1$  mV,  $1$  Hz square wave first increases and then decreases with the film thickness (Figure 2b). As the film thickness initially increases, more active sensing materials lead to a higher electrochromic contrast. However, when the film thickness continues to increase, the signal is limited by the penetration depth of the evanescent wave at the total-internal-reflection interface.<sup>32</sup> The experimental data agree very well with modeling results, with an optimal thickness  $\sim 65$  nm. For two-channel recordings, the sensitivity is usually higher for the 561 nm channel than the 658 nm channel since the extinction coefficient shows a stronger voltage dependence at 561 nm. Nevertheless, both the 561 nm channel and the 658 nm channel have good sensitivity to detect extracellular action potentials.

At angles above the critical angle of  $\sim 62.5^\circ$ , we find that the total reflectance  $R$  gradually increases with incident angle for both 561 and 658 nm lasers (Figure 2c). But, the signal  $\Delta R/R$  in response to a  $1$  mV square wave shows an optimal angle,  $\sim 68^\circ$  for 561 nm and  $\sim 67^\circ$  for 658 nm (Figure 2d). The experimental data also fits well with the modeling when using two different refractive indexes for two different wavelengths. Hence, for all our biological measurements, we set the incident angle as  $\sim 67.5^\circ$  to maintain good sensitivity for both recording channels.

The sensitivity of dual-color ECORE is strongly dependent on the bias potential applied to the film. We measured the total internal reflectance  $R$  and the signal  $\Delta R/R$  when different bias voltages were applied to the PEDOT:PSS film (Figure 2e).  $R$  increases with the bias potential for the 561 nm laser while decreases for the 658 nm laser. The changes are in the opposite directions compared to the UV–vis measurements (Figure 1c) because ECORE measures the reflection while UV–vis measures the absorption. For  $\Delta R/R$ , the recording sensitivity is high when the bias potential is less than  $-50$  mV. Nevertheless, both 561 and 658 nm channels show good sensitivity in optical responses at zero bias potential (Figure 2f).

Cell measurements are carried out in an open-circuit configuration with no electrode in the culture medium. Therefore, we measured the open circuit potential,  $E_{\text{open}}$ , for PEDOT:PSS films at different conditions (Figure 2g and Supporting Information). We found that the  $E_{\text{open}}$  of freshly electropolymerized PEDOT:PSS film is  $\sim 200$  mV (Day  $-1$ ) in an oxidized state.<sup>33</sup> Upon exposure to cell culture medium for 1 or more days,  $E_{\text{open}}$  decreases significantly and then stabilizes, likely due to the presence of reductive components in the cell culture medium. Our measurements show, in cell culture medium, PEDOT:PSS bare films having an  $E_{\text{open}}$  of  $-106$  mV, Matrigel-coated PEDOT:PSS films having an  $E_{\text{open}}$  of  $-71$  mV, and PEDOT:PSS film cultured with a cardiomyocyte monolayer showing an  $E_{\text{open}}$  of  $-34$  mV (Figure 2h). As shown in Figure 2f, the reductive culture environment ( $E_{\text{open}} \sim -40$  mV) enables better sensitivity for ECORE than zero bias.

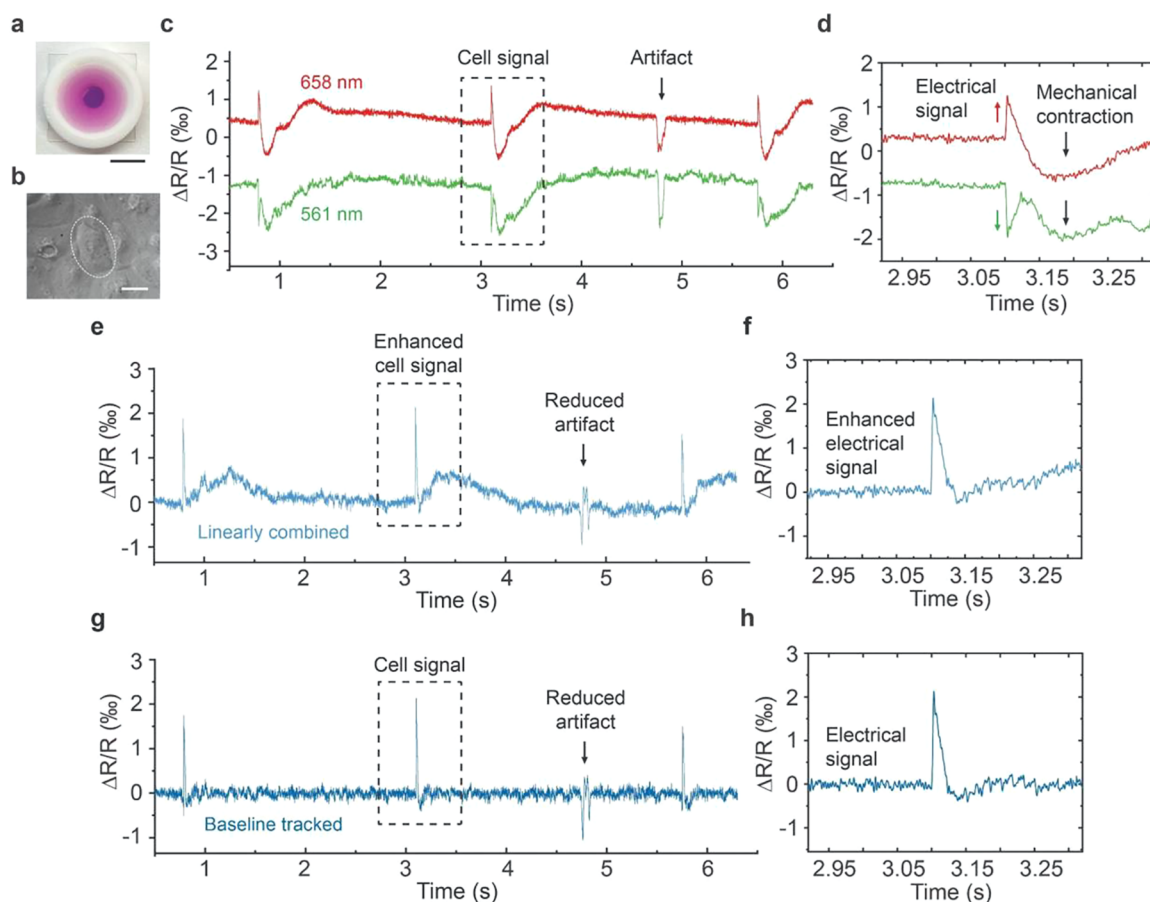


**Figure 3.** Dual-color ECORE of cardiomyocyte action potentials. (a) Photo of a cell culture device for ECORE measurement. Scale bar = 10 mm. (b) Monolayer of cardiomyocytes cultured on a PEDOT:PSS thin film at 11 days after seeding. The cell circled with a dashed line is selected for recording with dual-color ECORE. Scale bar = 50  $\mu\text{m}$ . (c) ECORE recording traces from the 561 nm channel (green) and the 658 nm channel (red). The cell signal is composed of electrical signals from cell action potentials (sharp spikes) followed by the mechanical signals from cell contraction (slower waves). The electrical signals appear in opposite polarity in two channels, while the mechanical contractions and an artifact signal appear in the same polarity. (d) Zoomed-in cell signals in the dash-line box in (c). (e) Linearly combined trace from two recording channels shows enhanced electrical signal and reduced baseline shift due to cell mechanical contraction. (f) Zoomed-in cell signals in the dashed box in e. (g) Baseline tracking algorithm was applied to flatten the baseline without affecting the electrical signals. (h) Zoomed-in electrical signals in the dash-line box in (g).

**Dual-Color ECORE Recording of Cardiomyocyte Action Potentials.** Using dual-color ECORE, we recorded action potentials from monolayers of human induced pluripotent stem cell-derived cardiomyocytes (hiPSC-cardiomyocytes). hiPSC-cardiomyocytes cultured on PEDOT:PSS thin films exhibit spontaneous and rhythmic contractions 2–3 days after seeding (Figure 3a). They can be maintained on the PEDOT:PSS thin films for two months or longer. Most of our recordings are performed 10–30 days after cell seeding when cells form a confluent monolayer and beat synchronously. These cardiomyocytes are large cells (50–100  $\mu\text{m}$  diameter), so we can use dual-color ECORE ( $\sim 25 \mu\text{m}$  probing beam) to probe single cells (Figure 3b).

Dual-color ECORE recordings from a cardiomyocyte show large and periodic signals associated with each beat (Figure 3c). A zoomed-in view of the signal shows a highly complex shape (Figure 3d). In cardiomyocytes, an electrical signal is immediately followed by a mechanical contraction through excitation-contraction coupling.<sup>17,19,22</sup> The mechanical contraction at the cell–substrate interface perturbs the light reflection and results in the complex ECORE signal. As shown in Figure 3d, the extracellular electrical signals appear as fast

spikes typically on the order of 5 ms, which can be easily distinguished by the opposite changes in the two channels (red and green arrows). This is because the PEDOT:PSS thin film shows opposite voltage-dependent spectral changes under 561 and 658 nm probing lasers. The mechanical signal, on the other hand, shows slow waves on the order of hundreds of milliseconds, which appear in the same direction in the two channels (black arrows). Likewise, an artifact in the recording trace (likely a dust particle) shows the same direction in the two-color channels. This is likely caused by a flying dust particle simultaneously blocking the spatially overlapping 561 and 658 nm probing lasers for a short period of time, which leads to a recording artifact in the same direction for both channels. This unique feature of dual-color ECORE allows us to distinguish electrical signals from mechanical motions, noises, or artifacts.

By combining signals from two color channels with appropriate linear coefficients, we are able to largely remove nonelectrical signals from cellular mechanical contraction and reduce artifacts as they are common modes to both channels (Figure 3e). In this way, the combined trace almost doubles the signal-to-noise ratio for electrical signals (Figure 3f). The

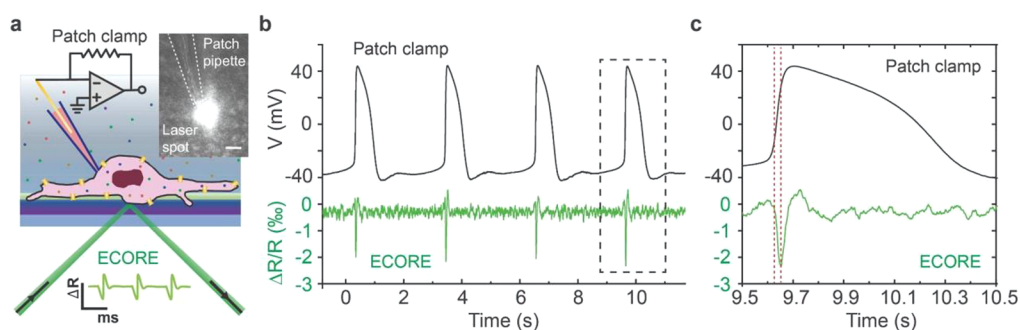


**Figure 4.** Simultaneous ECOPE and patch clamp recording. (a) Illustration of simultaneous ECOPE (single channel) and patch clamp recording. Inset: the probing laser spot and patch clamp pipette are focused onto the same cell. Scale bar = 50  $\mu\text{m}$ . (b) Synchronized recordings from patch clamp (intracellular action potentials) and from ECOPE (extracellular action potentials). (c) Zoomed-in intracellular and extracellular action potentials show that the extracellular spikes are time aligned to the sharp depolarization phase of the intracellular action potentials (dashed line).

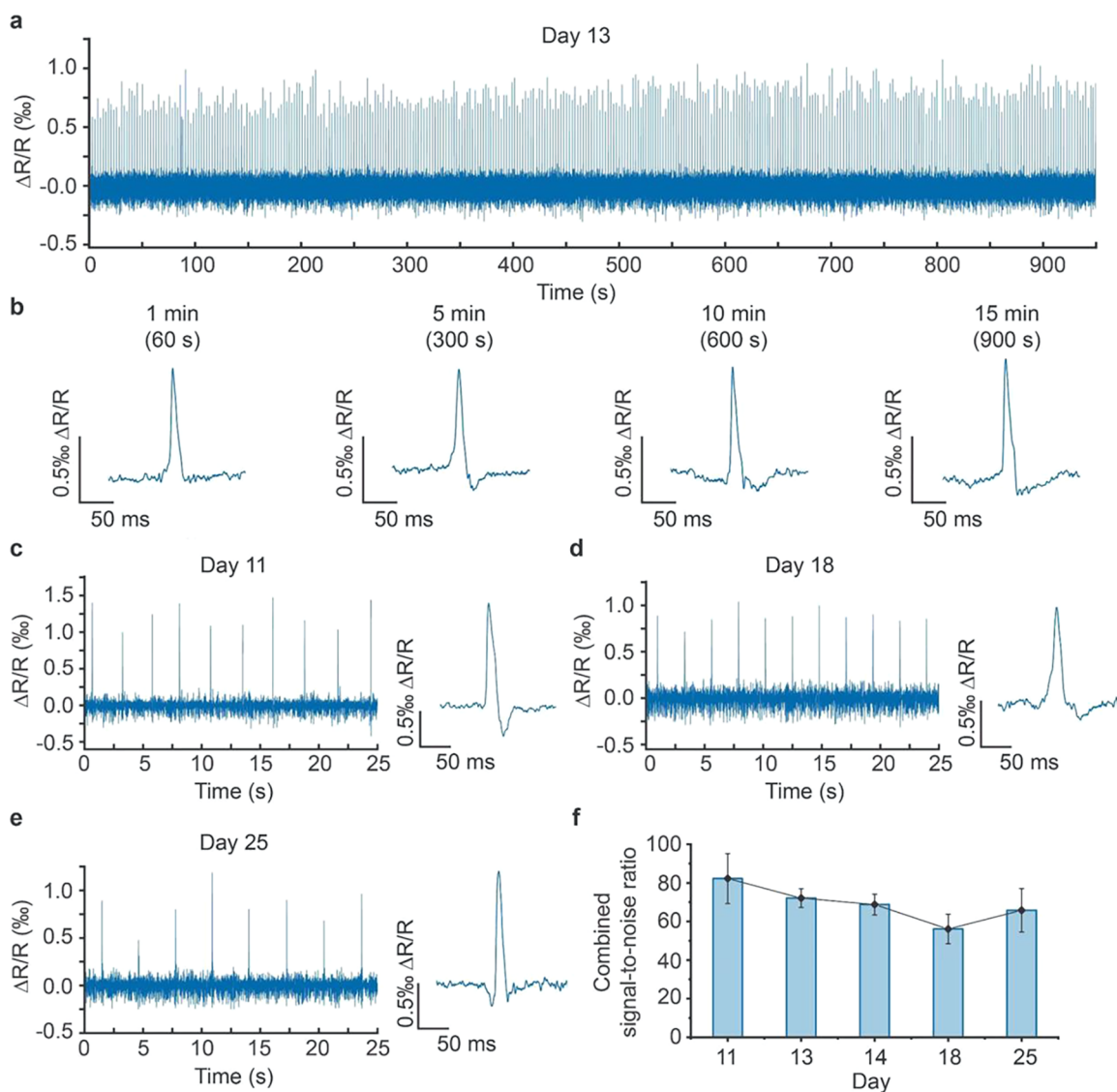


**Figure 5.** Stable and long-term recording of hiPSC-cardiomyocytes. (a) Fifteen minute dual-color recording (combined trace is shown) at 10 kHz frequency shows a stable recording of rhythmic action potentials from a cardiomyocyte at 13-day post seeding. (b) Zoomed-in traces at 1, 5, 10 and 15 min show that the optical signal amplitude does not decay over the long recording period. (c–e) Recording traces from the same culture at 11, 18, and 25 days after seeding on the PEDOT:PSS thin film. (f) Measured signal-to-noise ratios on different days. The signal-to-noise ratio is computed based on the average spike size over the standard deviation of the background noise at a 25 ms period. The error bar indicates two standard deviations.

slow waveform due to mechanical contraction is not completely removed as the light scattering differs slightly in the two-color channels. Finally, we applied a baseline tracking algorithm (Experimental Methods) to flatten out the small residue baseline fluctuation in the combined recording trace (Figure 3g,h). The advantage of dual-color ECORE is further demonstrated by examining different cells. As the mechanical signals are due to the perturbed light reflection at the cell–substrate interface, they could vary significantly depending on the cellular location and can appear as a peak upward, downward, or irregular up-and-down fluctuation (Figure S6a). Even though the mechanical signals may appear in different waveforms in the two channels, the electrical signals always remain in opposite polarity (Figure S6b) and can be clearly distinguished after combining the two traces and flattening out the baseline (Figure S6c,d).

**Simultaneous ECORE and Patch Clamp Recording Confirm Bioelectrical Signals.** The action potentials of hiPSC-cardiomyocytes measured from ECORE are further confirmed through a simultaneous ECORE and patch clamp recording experiment from the same cell (Figure 4a). It is important to note that the patch clamp electrode breaks through the cell membrane and accesses the cell interior to measure intracellular action potentials, while the electrochromic polymer film is located outside the cell membrane and measures extracellular action potentials. Electrical signals from the patch clamp amplifier and the green channel of the ECORE detector are digitized by the same digitizer to synchronize the time stamp. Time-aligned traces show that action potentials recorded from patch clamp aligns well with the extracellular action potentials measured from ECORE (Figure 4b). The traces show distinct waveforms of intracellular recordings and extracellular recordings from the same cell. The peak of the extracellular spike corresponds to the initial fast depolarization phase of the intracellular potential resulting from the opening of Na<sup>+</sup> channels (Figure 4c). This agrees with previous extracellular measurements by multi-electrode arrays.<sup>34,35</sup> The cardiomyocyte junctional membrane in contact with the electrochromic polymer film can be modeled as a resistor-capacitor circuit (RC circuit) that functions as a high pass filter.<sup>34–36</sup> As a result, the extracellular potential measured from ECORE is dominated by the fast depolarization phase signal resulting from the Na<sup>+</sup> channels.

**Long-Term Recording of Cardiomyocytes Using Dual-Color ECORE.** Figure 5a shows the combined dual-color recording trace of a single hiPSC-cardiomyocyte for >15 min. By linearly combining the two recording channels, large fluctuations due to cell mechanical contraction are largely eliminated for the entire time duration. The combined recording trace achieved a recording SNR of >50 for the extracellular action potential. As illustrated in the zoomed-in recording snapshots of a single action potential at 1, 5, 10, and 15 min(s) (Figure 5b), the shape and millisecond spiking of extracellular action potential are clearly resolved. Moreover, the recording SNR remains stable over the 15 min period (at 10 kHz recording frequency) without any sign of time-dependent degradation. The signal-to-noise ratio and the signal stability are much improved over voltage-sensitive fluorophores and single-channel ECORE.

We further performed long-term recordings of cardiomyocytes from the same culture over multiple days. Parts c–e of Figure 5 shows examples of the combined dual-color recording trace at 11, 18, and 25 days after cell seeding. The zoomed-in

snapshots again clearly resolve the shape and millisecond spiking of extracellular action potentials. The SNR fluctuates over different days but remains in an excellent range of 50–80 during the 25 day period (Figure 5f). This level of recording SNR is comparable to recordings from flat multielectrode arrays,<sup>34,37,38</sup> with the unique advantage of spatial flexibility offered by optical recording.

## DISCUSSION

Optical recording of bioelectrical signals possesses numerous advantages.<sup>39</sup> It avoids complex electrical wiring, offers spatial flexibility in selecting target cells and to image a network of cells, and has the potential to achieve high spatial resolution for subcellular detection. The key challenge of optical recording is to find an effective mechanism to convert bioelectrical signals into a stable optical readout. Previously, fluorescent labels were widely used to fulfill this purpose. Despite their significant advantages, fluorescent labels often suffer from photobleaching, low brightness, and sometimes phototoxicity upon long-duration recording.

This work reports on dual-color label-free optical recording that leverages polymer electrochromism to convert cell electrical signals into a stable reflection, rather than fluorescence, as optical readouts. Dual-color ECORE is complementary to fluorescence-based optical recording and would be suitable to study systems that require high-frequency and long-duration recording or systems that are sensitive to molecular perturbation or difficult to genetically modify. The unique electrochromic property of PEDOT:PSS, where an electrical potential causes opposite optical changes at two different wavelengths, allows us to distinguish bioelectrical signals from recording noises and artifacts. The linear combination of dual-color recording traces also allows selective enhancement of electrical signals while suppressing baseline shift due to cell mechanical contraction.<sup>40</sup> Using dual-color ECORE, we recorded iPSC-cardiomyocytes with high signal quality, long recording duration, and without time-dependent signal degradation. We were also able to record from the same device over many days.

Nevertheless, a number of aspects can be further improved by future developmental efforts. For example, we expect that the sensitivity of dual-color ECORE can be enhanced by optimizing the laser wavelengths. The spatial resolution could be further improved by reducing the spot size of the probing lasers, and the recording throughput can also be increased from single-site recording of one cell to multisite recording of many cells by fast scanning the probing laser beams. Besides optical improvements, chemical improvements of detection sensitivity can be achieved by employing new materials with improved electrochromic properties.<sup>41,42</sup> These future efforts will make progress toward a new and versatile electrophysiology method in the future.

## EXPERIMENTAL METHODS

**Device Fabrication and Electropolymerization.** Indium tin oxide (ITO) coated glass slides (25 × 25 × 0.4 mm<sup>3</sup>) with resistance  $R_s = 70–100 \Omega$  (Surplus Part No. X260, Delta Technologies) were first cleaned with dish soap in a sonicator bath for 5 min. They were then dried and cleaned using a UV-ozone cleaner (UV-1, Samco) at 60 °C for 3 min and 30 s. Custom 3-D printed poly(lactic acid) (PLA) sample wells with a circular bottom opening of Ø6 mm were glued onto the ITO coated glass slides using RTV108 silicone glue (Momentive) and were allowed to cure for 24–72 h. Aqueous

solution (19.58 mL) containing 0.4 g (2 w/w%) of poly(sodium 4-styrenesulfonate) (PSS) ( $M_w = 70,000$ , SigmaAldrich) was mixed with 20  $\mu\text{L}$  of 3,4-ethylenedioxythiophene (EDOT) (SigmaAldrich) to make a 10 mM solution. The solution was allowed to equilibrate overnight and filtered using a 1.2  $\mu\text{m}$  syringe filter. One milliliter of filtered EDOT:PSS solution was then added to the sample well, and electropolymerization was conducted by applying a constant voltage of 950 mV to the ITO coated glass with respect to the Ag/AgCl reference electrode using a potentiostat (SP-200, BioLogic) and based on a three-electrode cell setup. In this way, a PEDOT:PSS thin film with an area of 28.3  $\text{mm}^2$  was deposited on the ITO coated glass. The film thickness was controlled by varying the electropolymerization time. For example, a 60 s electrodeposition time results in  $\sim 65$  nm film thickness.

**UV-vis Spectroscopy.** A custom designed, 3-D printed cuvette that simultaneously fits the sample, the Ag/AgCl reference electrode (RE6, BASi Research Products), and the platinum counter electrode was placed in the sample chamber of a UV-vis spectrophotometer (Lambda 25, PerkinElmer). The position of the cuvette in the sample chamber was carefully adjusted to ensure that the probing beam passed through the center of the PEDOT:PSS thin film. The UV-vis spectrometer scans from 300 to 800 nm with a 1 nm step. During the measurement, the cuvette was filled with HEPES (4-(2-hydroxyethyl)-1-piperazineethanesulfonic acid) buffered Tyrode's salt solution and a potentiostat (SP-200, BioLogic) was used to apply the biasing voltage to the PEDOT:PSS thin film from +600 to -700 mV with a 100 mV step.

**Thickness and Surface Characterization of PEDOT:PSS Films.** The glued sample well on the ITO glass was first removed using a razor blade. Next, a blunt tip tweezer or a pipet tip was used to gently scratch near the center of the PEDOT:PSS thin film. The thickness of the PEDOT:PSS thin film was measured using a Bruker Dektak XT profilometer (Bruker Corporation). For each sample, five measurements were performed and the average film thickness was calculated. The surface morphology of the PEDOT:PSS thin film was imaged using a Bruker Dimension Icon atomic force microscope (AFM) (Bruker Corporation) under the peak force tapping mode using an NSC19/Al BS AFM probe (Mikromasch).

**Optical Setup of Dual-Color ECORE.** A 20 mW, 658 nm laser diode pigtailed with a single-mode fiber (LP660-SF20, Thorlabs) was mounted on a temperature-controlled laser diode mount (LDM56, Thorlabs) equipped with a current and temperature controller. The 658 nm laser beam was directed through an optical isolator (ISO-04-650-MP, Newport) and coupled into a single mode optical fiber (P3-460B-FC-2, Thorlabs). A 50 mW, 561 nm diode-pumped solid-state laser (Excelsior, Spectra Physics) was directed through a 0.3 (50%) and a 0.1 (79%) neutral density filters and coupled into the same single mode optical fiber as the 658 nm laser. In this way, the two laser beams were spatially overlapped coming out of the fiber coupling port. The polarization of the two overlapping laser beams was then adjusted using an achromatic half-wave plate (AHWP05M-600, Thorlabs) and filtered by a polarizing beam splitter cube (PBS201, Thorlabs). The filtered beams were again directed through an 830 nm half-wave plate (WPH05M-830, Thorlabs) and an achromatic half-wave plate (AHWP05M-600, Thorlabs). The two half-wave plates were chosen to have different optical retardances to 561 and 658 nm lasers so that the polarization of the two laser beams could be independently adjusted while remaining spatially overlapped. A second polarized beam splitter cube (PBS101, Thorlabs) then separated the polarized overlapping beams into two orthogonal linearly polarized overlapping beams. The amount of *p*- and *s*-polarization was manually controlled by the preceding two half-wave plates. Next, one overlapping beam that served as the sample beam was directed through a third achromatic half-wave plate (AHWP10M-600, Thorlabs), after which the beam polarization was adjusted to *s*-polarized and was focused to the prism. Here, a 20 mm BK-7 equilateral prism (24-2158-000, Ealing Catalog) was placed on a custom 3-D printed prism holder mounted to a rotational stage (CRL1, Thorlabs) such that the incident angle can be tuned by adjusting the prism angle. The rotational stage was held by an XYZ linear

translational stage (9064-XYZ, Newport) such that the position of the prism can also be adjusted. Here, light refraction causes only negligible beam displacement between the two wavelengths as the beam enters the equilateral prism nearly orthogonally to the surface. For example, an incident angle of  $67^\circ$  relative to the PEDOT:PSS film surface is expected to have  $<1$   $\mu\text{m}$  displacement if the path through the glass is 10 mm. The sample beam was then collected and split by a 625 nm long-pass dichroic mirror into 561 and 658 nm beams. The other pair of overlapping beams served as the reference beams and were directly split into 561 and 658 nm beams by a 612 nm long-pass dichroic mirror. Finally, the split dual-color sample and reference beams were directed to their own relative differential photodetectors. A 20 $\times$  long working distance objective (378-824, Mitutoyo) was connected to a CCD camera (DMK41BF02.H, ImagingSource) was mounted on top of the prism for brightfield imaging of the sample well. During dual-color ECORE measurement, both balanced differential photodetectors of the 561 and 658 nm channels reject laser intensity noise by comparing the reflected beam from the cell sample against the reference beam derived from the same laser.<sup>22</sup> In this way, background laser noise is removed from the sample beam to further reduce the recording noise.

**Beam Spot Size Characterization.** The intensity of the laser beam was first attenuated using neutral density filters such that it did not saturate the CCD camera. The CCD camera was then used to image the laser beam spot. ImageJ software was used to determine the laser spot intensity profile, which was fitted based on a Gaussian distribution. The measured full width at half-maximum (fwhm) was used to determine the laser spot diameter,  $D$ , defined as

$$D = 2 \times \frac{\text{FWHM}}{\sqrt{2 \ln 2}}$$

The pixel size of the camera under 20 $\times$  objective was also calibrated using a microscope eyepiece ruler and found to be 0.349  $\mu\text{m}/\text{pixel}$ .

**Data Acquisition Using Dual-Color ECORE.** Before each recording, the cell culture media was replaced with 200  $\mu\text{L}$  of HEPES buffered Tyrode's solution at 37  $^\circ\text{C}$ . A thin layer of Type F immersion oil ( $n_0 = 1.518$ , Leica) was applied to the bottom of the ITO glass for index matching with the prism and suppression of the back reflection from the ITO glass. The two overlapping probing beams (561 and 658 nm) were focused onto the cell of interest. For each recording channel, the sample and the reference beams were directed to the photodiodes of the two homemade differential photodiode detectors, which convert optical signals into voltage signals. The voltage outputs for the 561 nm channel and the 658 nm channel were both filtered using 10 kHz low-pass electrical filters (EF120, Thorlabs) before being amplified using two patch clamp amplifiers (Axopatch-1A, Molecular Devices). The amplified output from the amplifiers are then connected to homemade Bessel filters (8 and 17 kHz) to filter out the amplifier noise. The filtered amplified signals from both channels were then separately digitized at 10 kHz rate using the same low-noise digitizer (Axon Digidata 1440A, Molecular Devices) to ensure synchronization. Data was recorded using Clampex 10 software. Before the start of each recording, the light intensities of the sample beam and the reference beam reaching the differential photodetectors were manually adjusted to be approximately the same by rotating the two half-wave plates in the light path. In this way, the differential photodetectors were "balanced" in order to maximize the recording dynamic range for reflectance change  $\Delta R$  (in volts). The powers of the laser beams reaching the differential photodetectors from the sample arm and the reference arm (in  $\mu\text{W}$ ) were also separately measured using a photodiode power sensor (S120C, Thorlabs) connected to an optical power meter (PM100D, Thorlabs), which give the values for reflectivity  $R$ .

**Data Analysis.** The reflectance  $R$  was calculated by dividing the power (in  $\mu\text{W}$ ) of the light reflected by the PEDOT:PSS film by the incident laser power (in mW) into the PEDOT:PSS film through the prism. The reflectance change  $\Delta R$  (in volts) was converted into fractional reflectance change  $\Delta R/R$  with respect to the reflected laser power reaching the photodiodes of the differential photodetector. All laser power was measured using an optical power meter. Since the

photodiode converts light into electrical signal, the reflectance change  $\Delta R/R$  is defined as

$$\Delta R/R = \Delta R / (\text{responsivity} \times \text{feedback resistance} \\ \times \text{reflected laser power} \times \text{amplifier gain})$$

The responsivity varies depending on the photodiode and the laser wavelength. For the 561 nm channel, the responsivity is 0.232 A/W for the photodiode (FDS100, Thorlabs) used in the differential photodetector. For the 658 nm channel, the responsivity is 0.46 A/W for the photodiode used (FND-100, Excelitas). The feedback resistor resistance in the differential photodetectors is 100 k $\Omega$ . The gain was set to 100 $\times$  for cell measurements and 50 $\times$  for cell-free square-wave measurements.

All the raw data was first filtered using a notch-filter with a  $-3$  dB cutoff frequency at 60 Hz to remove electrical noise up to the seventh harmonic. The low-pass filter applied was a third order Butterworth filter at a cutoff frequency of 280 Hz. For simultaneous ECORE and patch clamp measurement only, an additional first order Butterworth high-pass filter at a cutoff frequency of 10 Hz was applied in order to remove the baseline shift due to cell mechanical contraction. Digital filters were implemented through Python.

The baseline tracking of cardiomyocytes recording traces was done by an 800th-order 1-D median filtering function implemented through Matlab. The median filtering algorithm tracks the remaining slow baseline shift in the linearly combined recording trace but lets the fast bioelectrical signals pass. The tracked baseline profile was then subtracted from the combined recording trace to fully flatten the combined recording baseline.

The signal-to-noise ratio (SNR) of the square-wave potential and action potential for each channel is calculated as the spike height divided by the baseline noise. Spike height of the action potential was determined through a peak-finding algorithm in Python and averaged over multiple spikes in the recording traces for reliable statistics. The baseline noise was determined by zooming into the recording baseline that is relatively flat and then computing the standard deviation of a 25 ms baseline before or after the action potential spikes.

The weighted average SNR of the two recording channels for square-wave potential response is calculated as  $\overline{\text{SNR}} = \sqrt{\text{SNR}_{561\text{nm}}^2 + \text{SNR}_{658\text{nm}}^2}$  when the noise in both channels is uncorrelated. The individual weight for the 561 nm channel  $w_{561\text{nm}} = \frac{\text{SNR}_{561\text{nm}}^2}{\text{SNR}_{561\text{nm}}^2 + \text{SNR}_{658\text{nm}}^2}$ , and the individual weight for the 658 nm channel  $w_{658\text{nm}} = \frac{\text{SNR}_{658\text{nm}}^2}{\text{SNR}_{561\text{nm}}^2 + \text{SNR}_{658\text{nm}}^2}$ .

**Simultaneous ECORE and Patch Clamp Recording.** Simultaneous ECORE and patch clamp recordings were carried out on hiPSC-cardiomyocytes at room temperature in HEPES buffered Tyrode's salt solution. The patch clamp head stage was mounted near the ECORE prism stage such that the patch clamp pipettes could access the cells in the ECORE sample well. During the experiments, a laser spot is first focused onto the cell of interest. After an extracellular action potential was measured through ECORE, the laser was temporarily turned off and the same cell was patched. After an intracellular action potential signal was measured through the patch clamp, the laser was turned back on for simultaneous ECORE and patch clamp recording. To ensure synchronized recording between ECORE and patch clamp, the same low-noise digitizer (Axon Digidata 1440A, Molecular Devices) was connected to the ECORE and patch clamp output channel. For ECORE, single-color recording mode using a 532 nm laser was used and a bandpass filter was applied. For patch clamp, the action potential was recorded under whole-cell current-clamp mode using a Multiclamp 700B amplifier (Axon Instrument) with Clampex 10 software (Molecular Device). Borosilicate patch pipettes (O.D. 1.5 mm, I.D. 0.86 mm, Sutter Instrument) were pulled with a P1000 pipet puller (Sutter Instrument) with resistances between 2 and 6 M $\Omega$ . Pipette internal solution contained 20 mM potassium aspartate, 20 mM KCl, 1 mM MgCl<sub>2</sub>, 5 mM EGTA-KOH, 0.1 mM CaCl<sub>2</sub>, 10 mM HEPES, and 4

mM Mg<sub>2</sub>ATP. The pH was adjusted to 7.2 with KOH. The patch clamp recording was performed at 10 kHz sampling rate with an applied 10 kHz Bessel filter.

**Culturing of hiPSC-cardiomyocytes.** hiPSC-derived cardiomyocytes were maintained in Matrigel precoated 6-well plates in RPMI 1640 media (Gibco REF 11875-093, 500 mL) with B-27 supplement (Gibco REF 17504-044, 10 mL). The culture media was refreshed every 2–3 days. Before seeding cells on the device with PEDOT:PSS thin films, the device was first disinfected with 70% EtOH for 30 min, followed by rinsing three times with 1 $\times$  PBS solution. The PEDOT:PSS film was then coated with 1 mg/mL poly-L-lysine in PBS for 30 min at room temperature and then rinsed three times with 1 $\times$  PBS solution. The PEDOT:PSS film was then coated with 0.5% glutaraldehyde in 1 $\times$  PBS for 15 min at room temperature followed by another three-time rinsing with 1 $\times$  PBS. Next, the PEDOT:PSS film was coated with 1:200 Matrigel (Corning REF 356231) in DMEM/F12 (Gibco REF 10565-018) at 37  $^{\circ}$ C for 1 h. Cells were dissociated with TryPLE select 10 $\times$  (Gibco REF A12177-01) at 37  $^{\circ}$ C for 5 min from the 6-well plate and  $\sim 1.2 \times 10^5$  cells were plated in each coated PEDOT:PSS device in culture media supplemented with 10% KnockOut Serum Replacement (KSR) (Gibco REF A31815-01), and cultured in 5% CO<sub>2</sub> incubator at 37  $^{\circ}$ C. The media was refreshed with normal culture media every 2 days from the second day after replating. Recordings from cardiomyocytes typically start on Day 10 after cell seeding.

## ■ ASSOCIATED CONTENT

### Supporting Information

The Supporting Information is available free of charge at <https://pubs.acs.org/doi/10.1021/jacs.2c10198>.

Discussions of modeling the light reflection at the glass/ITO/PEDOT/water interface, and open circuit potential of PEDOT:PSS film and figures of electro-polymerized PEDOT:PSS thin film thickness as a function of electropolymerization time, AFM image, UV–vis spectra under different applied voltages, optical setup of two-color ECORE, two probing lasers of and focused to the prism, fractional reflectance change  $\Delta R/R$  of a  $\sim 60$  nm PEDOT:PSS thin film, and cell signals from a different hiPSC-cardiomyocyte (PDF)

## ■ AUTHOR INFORMATION

### Corresponding Authors

**Bianxiao Cui** – Department of Chemistry and Wu Tsai Neurosciences Institute, Stanford University, Stanford, California 94305, United States; [orcid.org/0000-0002-8044-5629](https://orcid.org/0000-0002-8044-5629); Email: [bcui@stanford.edu](mailto:bcui@stanford.edu)

**Holger Müller** – Department of Physics, University of California, Berkeley, California 94720, United States; Molecular Biophysics and Integrated Bioimaging, Lawrence Berkeley National Laboratory, Berkeley, California 94720, United States; Email: [hm@berkeley.edu](mailto:hm@berkeley.edu)

### Authors

**Yuecheng Zhou** – Department of Chemistry, Stanford University, Stanford, California 94305, United States; [orcid.org/0000-0002-3105-7697](https://orcid.org/0000-0002-3105-7697)

**Erica Liu** – Department of Chemistry, Stanford University, Stanford, California 94305, United States; [orcid.org/0000-0002-1193-0049](https://orcid.org/0000-0002-1193-0049)

**Yang Yang** – Department of Chemistry, Stanford University, Stanford, California 94305, United States

**Felix S. Alfonso** – Department of Chemistry, Stanford University, Stanford, California 94305, United States

Burhan Ahmed – Department of Physics, University of California, Berkeley, California 94720, United States; [orcid.org/0000-0003-4379-7809](https://orcid.org/0000-0003-4379-7809)

Kenneth Nakasone – Department of Physics, University of California, Berkeley, California 94720, United States

Csaba Forró – Department of Chemistry, Stanford University, Stanford, California 94305, United States

Complete contact information is available at:

<https://pubs.acs.org/10.1021/jacs.2c10198>

## Notes

The authors declare no competing financial interest.

## ACKNOWLEDGMENTS

The authors thank Professor Steven Boxer for the access of the digitizer and UV–vis spectrophotometer in his lab and Jacob Kirsh for helping set up these equipment. The authors thank Sarah Jones and Caravaggio Caniglia for helping with the design of UV–vis cuvettes and UV–vis measurements. The authors thank Professor Joseph Wu for providing the hiPSC-Cardiomyocytes cell line. The authors thank Dr. Wei Zhang, Professor Zeinab Jahed and Professor Xiao Li for inspiring discussions. This work was financially supported by the National Institutes of Health grant No. 1R01NS121934-01, the David and Lucile Packard Foundation (B.C. and H.M.), and the NIH Stanford Graduate Training Program in Biotechnology T32GM141819 (E.L.). Part of this work was performed at the Stanford Nano Shared Facilities (SNSF), supported by the National Science Foundation under award ECCS-2026822.

## REFERENCES

- (1) Colatsky, T.; et al. The Comprehensive in Vitro Proarrhythmia Assay (CiPA) initiative - Update on progress. *J. Pharmacol. Toxicol. Methods* **2016**, *81*, 15–20.
- (2) Adam, Y.; et al. Voltage imaging and optogenetics reveal behaviour-dependent changes in hippocampal dynamics. *Nature* **2019**, *569*, 413–417.
- (3) Musk, E.; Neuralink. An integrated brain-machine interface platform with thousands of channels. *J. Med. Internet. Res.* **2019**, *21* (10), e16194.
- (4) Scanziani, M.; Häusser, M. Electrophysiology in the age of light. *Nature* **2009**, *461*, 930–939.
- (5) Wilt, B. A.; et al. Advances in light microscopy for neuroscience. *Annu. Rev. Neurosci.* **2009**, *32*, 435–506.
- (6) Yang, H. H.; et al. Subcellular Imaging of Voltage and Calcium Signals Reveals Neural Processing In Vivo. *Cell* **2016**, *166*, 245–257.
- (7) Tian, L.; et al. Imaging neural activity in worms, flies and mice with improved GCaMP calcium indicators. *Nat. Methods* **2009**, *6*, 875–881.
- (8) Grienberger, C.; Konnerth, A. Imaging calcium in neurons. *Neuron* **2012**, *73*, 862–885.
- (9) Chen, T.-W.; et al. Ultrasensitive fluorescent proteins for imaging neuronal activity. *Nature* **2013**, *499*, 295–300.
- (10) Miller, E. W. Small molecule fluorescent voltage indicators for studying membrane potential. *Curr. Opin. Chem. Biol.* **2016**, *33*, 74–80.
- (11) Xu, Y.; Zou, P.; Cohen, A. E. Voltage imaging with genetically encoded indicators. *Curr. Opin. Chem. Biol.* **2017**, *39*, 1–10.
- (12) Grandy, T. H.; Greenfield, S. A.; Devonshire, I. M. An evaluation of in vivo voltage-sensitive dyes: pharmacological side effects and signal-to-noise ratios after effective removal of brain-pulsation artifacts. *J. Neurophysiol.* **2012**, *108*, 2931–2945.
- (13) Hirase, H.; Nikolenko, V.; Goldberg, J. H.; Yuste, R. Multiphoton stimulation of neurons. *J. Neurobiol.* **2002**, *51*, 237–247.
- (14) Mennerick, S.; et al. Diverse voltage-sensitive dyes modulate GABAA receptor function. *J. Neurosci.* **2010**, *30*, 2871–2879.
- (15) Maclaurin, D.; Venkatachalam, V.; Lee, H.; Cohen, A. E. Mechanism of voltage-sensitive fluorescence in a microbial rhodopsin. *Proc. Natl. Acad. Sci. U. S. A.* **2013**, *110*, 5939–5944.
- (16) Barry, J. F.; et al. Optical magnetic detection of single-neuron action potentials using quantum defects in diamond. *Proc. Natl. Acad. Sci. U. S. A.* **2016**, *113*, 14133–14138.
- (17) Balch, H. B.; et al. Graphene Electric Field Sensor Enables Single Shot Label-Free Imaging of Bioelectric Potentials. *Nano Lett.* **2021**, *21*, 4944–4949.
- (18) Zhou, Y.; Liu, E.; Müller, H.; Cui, B. Optical Electrophysiology: Toward the Goal of Label-Free Voltage Imaging. *J. Am. Chem. Soc.* **2021**, *143*, 10482–10499.
- (19) Bers, D. M. Cardiac excitation–contraction coupling. *Nature* **2002**, *415*, 198–205.
- (20) Habib, A.; et al. Electro-plasmonic nanoantenna: A non-fluorescent optical probe for ultrasensitive label-free detection of electrophysiological signals. *Sci. Adv.* **2019**, *5* (10), eaav9786.
- (21) Beaujuge, P. M.; Reynolds, J. R. Color control in pi-conjugated organic polymers for use in electrochromic devices. *Chem. Rev.* **2010**, *110*, 268–320.
- (22) Alfonso, F. S.; et al. Label-free optical detection of bioelectric potentials using electrochromic thin films. *Proc. Natl. Acad. Sci. U. S. A.* **2020**, *117*, 17260–17268.
- (23) Lang, U.; Müller, E.; Naujoks, N.; Dual, J. Microscopical Investigations of PEDOT:PSS Thin Films. *Adv. Funct. Mater.* **2009**, *19*, 1215–1220.
- (24) Mortimer, R. J. Electrochromic Materials. *Annu. Rev. Mater. Res.* **2011**, *41*, 241–268.
- (25) Makula, P.; Pacia, M.; Macyk, W. How To Correctly Determine the Band Gap Energy of Modified Semiconductor Photocatalysts Based on UV-Vis Spectra. *J. Phys. Chem. Lett.* **2018**, *9*, 6814–6817.
- (26) Cutler, C. A.; Bouguettaya, M.; Reynolds, J. R. PEDOT Polyelectrolyte Based Electrochromic Films via Electrostatic Adsorption. *Adv. Mater.* **2002**, *14*, 684–688.
- (27) Nowak, A. P.; Wilamowska, M.; Lisowska-Oleksiak, A. Spectroelectrochemical characteristics of poly(3,4-ethylenedioxythiophene)/iron hexacyanoferrate film-modified electrodes. *J. Solid State Electrochem.* **2010**, *14*, 263–270.
- (28) Im, S. G.; Gleason, K. K. Systematic Control of the Electrical Conductivity of Poly(3,4-ethylenedioxythiophene) via Oxidative Chemical Vapor Deposition. *Macromolecules* **2007**, *40*, 6552–6556.
- (29) Gribkova, O. L.; et al. The influence of polyacid nature on poly(3,4-ethylenedioxythiophene) electrosynthesis and its spectroelectrochemical properties. *J. Solid State Electrochem.* **2016**, *20*, 2991–3001.
- (30) Kabanova, V.; Gribkova, O.; Nekrasov, A. Poly(3,4-ethylenedioxythiophene) Electrosynthesis in the Presence of Mixtures of Flexible-Chain and Rigid-Chain Polyelectrolytes. *Polymers* **2021**, *13*, 3866.
- (31) Koutsouras, D. A.; et al. Impedance Spectroscopy of Spin-Cast and Electrochemically Deposited PEDOT:PSS Films on Micro-fabricated Electrodes with Various Areas. *ChemElectroChem.* **2017**, *4*, 2321–2327.
- (32) Fish, K. N. Total Internal Reflection Fluorescence (TIRF) Microscopy. *Current Protocols* **2022**, *2*, e517.
- (33) Zozoulenko, I.; et al. Polarons, Bipolarons, And Absorption Spectroscopy of PEDOT. *ACS Appl. Polym. Mater.* **2019**, *1*, 83–94.
- (34) Xie, C.; Lin, Z.; Hanson, L.; Cui, Y.; Cui, B. Intracellular recording of action potentials by nanopillar electroporation. *Nat. Nanotechnol.* **2012**, *7*, 185–190.
- (35) Dipalo, M.; et al. Intracellular and Extracellular Recording of Spontaneous Action Potentials in Mammalian Neurons and Cardiac Cells with 3D Plasmonic Nanoelectrodes. *Nano Lett.* **2017**, *17*, 3932–3939.
- (36) Spira, M. E.; Hai, A. Multi-electrode array technologies for neuroscience and cardiology. *Nat. Nanotechnol.* **2013**, *8*, 83–94.

(37) Lin, Z. C.; Xie, C.; Osakada, Y.; Cui, Y.; Cui, B. Iridium oxide nanotube electrodes for sensitive and prolonged intracellular measurement of action potentials. *Nat. Commun.* **2014**, *5*, 3206.

(38) Liu, Y.; et al. Soft conductive micropillar electrode arrays for biologically relevant electrophysiological recording. *Proc. Natl. Acad. Sci. U. S. A.* **2018**, *115*, 11718–11723.

(39) Knöpfel, T.; Song, C. Optical voltage imaging in neurons: moving from technology development to practical tool. *Nat. Rev. Neurosci.* **2019**, *20*, 719–727.

(40) Vinegoni, C.; Lee, S.; Aguirre, A. D.; Weissleder, R. New techniques for motion-artifact-free in vivo cardiac microscopy. *Front. Physiol.* **2015**, *6*, 147.

(41) Zhou, Y.; et al. Concentration-Driven Assembly and Sol-Gel Transition of  $\pi$ -Conjugated Oligopeptides. *ACS Cent Sci.* **2017**, *3*, 986–994.

(42) Advincula, A. A.; et al. Probing Comonomer Selection Effects on Dioxythiophene-Based Aqueous-Compatible Polymers for Redox Applications. *Chem. Mater.* **2022**, *34*, 4633–4645.